Discretized evolution of solitons in the achiral stripe phase of a Fe/Gd thin film

A. Singh [1,2] M. K. Sanyal [1,*] J. C. T. Lee,[2,3] J. J. Chess,[4] R. Streubel,[2,5,6] S. A. Montoya,[7] M. K. Mukhopadhyay [1]
B. J. McMorran [4] E. E. Fullerton,[7] P. Fischer [2,8] S. D. Kevan [2,3,4] and S. Roy [3,8,†]

[1]*Surface Physics and Material Science Division, Saha Institute of Nuclear Physics, HBNI, Kolkata, West Bengal 700064, India*
[2]*Materials Sciences Division, Lawrence Berkeley National Laboratory, Berkeley, California 94720, USA*
[3]*Advanced Light Source, Lawrence Berkeley National Laboratory, Berkeley, California 94720, USA*
[4]*Department of Physics, University of Oregon, Eugene, Oregon 97401, USA*
[5]*Department of Physics and Astronomy, University of Nebraska-Lincoln, Lincoln, Nebraska 68588, USA*
[6]*Nebraska Center for Materials and Nanoscience, University of Nebraska-Lincoln Lincoln, Nebraska 68588, USA*
[7]*Center for Memory and Recording Research, University of California San Diego, La Jolla, California 92093, USA*
[8]*Department of Physics, University of California, Santa Cruz, California 95064, USA*

Understanding magnetic phase transitions from stripe to skyrmion textures provide fundamental scientific insights into the details of the intermediate topologies through which the system evolves. The solitonic nature of spin texture in both stripe and skyrmion phases has been observed in materials with Dzyaloshinskii-Moriya interaction. Here we show that the field evolution in a dipolar interaction mediated Fe/Gd multilayer that exhibits achiral stripe textures behaves similar to a finite-sized chiral soliton lattice. As a function of magnetic field, the stripes exhibit discrete jumps in periodicity indicative of intermediate topologies as the stripes get wound into skyrmions.

I. INTRODUCTION

Solitons appear in diverse areas, such as hydrodynamics, optical communications, biological molecules, and magnetism, are solutions to nonlinear or coupled field equations and lead to stable particles, such as kinks, wave forms, or envelopes in various dimensions. A characteristic feature of those particlelike solitons is their topological structure [1–5], which has recently become an interesting topic for magnetic materials. In magnetic systems, domain wall, spin kinks, vortices that separate two different magnetic states, or incommensurate structures are among such examples of solitons [6–12]. Mathematically, soliton states can be described and quantified by the sine-Gordon equation, which is a common solution to physical processes involving periodic potentials with a complex order parameter. In cases where the system crosses different topological sectors the order parameter can show discrete jumps [13–16].

The solitonic nature of spin textures has been studied extensively in chiral magnetic systems, for example, in $CrNb_3S_3$ [6,14] where the chiral structure originates from the antisymmetric exchange interaction, i.e., the Dzyaloshinskii-Moriya interaction (DMI). This type of chiral magnetic order shows a higher level of coherence and stability. In contrast to the symmetric exchange interaction, which is expressed by the scalar product between two neighboring spins $\mathbf{S}_i$ and $\mathbf{S}_j$ and leads to a parallel or antiparallel alignment in the energetic ground state, the DMI is expressed as $\mathbf{D} \cdot \mathbf{S}_i \times \mathbf{S}_j$ that results in a twist between the ith and jth spins. The directionality of the chirality comes from the DM-vector $\mathbf{D}$ [17].

We have shown here that soliton physics [6,7], which has been successfully used to describe evolution of stripe phase in single crystals exhibiting DM interaction, can also explain variation of intensity and periodicity of magnetic Bragg peaks measured by x-ray scattering as a function of temperature and magnetic field in non-DMI amorphous thin films having dominant dipole interactions [6,16]. The presented results clearly show the existence of the one-dimensional chiral soliton lattice (1D-CSL) of finite size in a dipolar mediated amorphous thin film. As theoretically predicted discrete jumps in stripe periodicity and intensity variation of first- and second-order stripe diffraction peaks is observed. Such variation has been observed earlier in DMI systems that form a chiral helimagnet having fixed boundary conditions with a magnetic field applied perpendicular to the chiral axis [6,7,14,16]. The spatial mixing of these local chiralities gets averaged out to generate achiral nature in dipolar films. Interestingly by tuning the field and temperature we show that stripe-to-skyrmion phase transition has profound effects on the magnetic Bragg peaks as the system evolves from 1D-CSL to the two-dimensional skyrmion lattice (2D-SkL).

II. METHODS

We have used here an achiral dipolar mediated amorphous Fe/Gd multilayer film ([Gd (0.4 nm)/Fe (0.34 nm)] × 80 multilayers) which exhibits an aligned stripe, a disordered stripe, a skyrmion, and skyrmion bound-pair

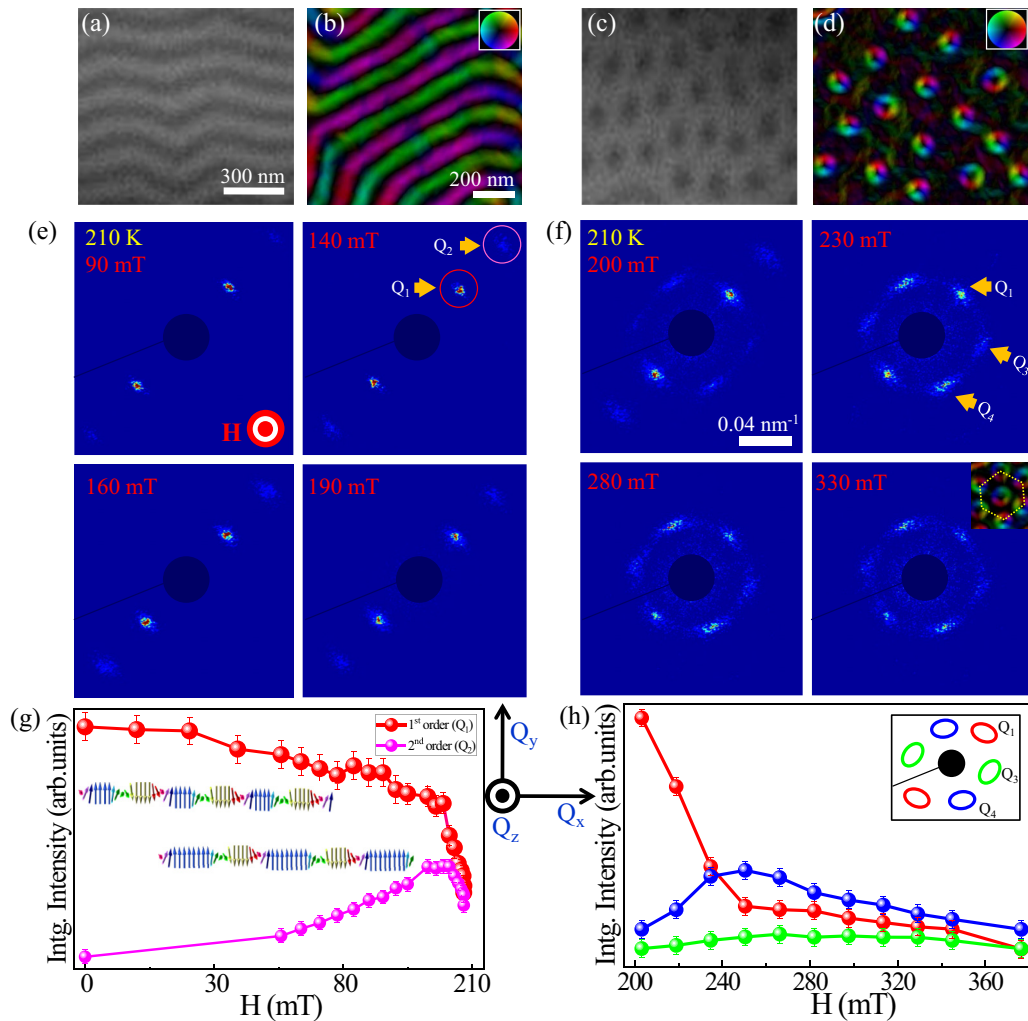*milank.sanyal@saha.ac.in
†sroy@lbl.gov

FIG. 1. Real-space data of magnetic spin stripes and skyrmions in a Fe/Gd multilayer using (a) and (c) magnetic full-field transmission x-ray microscopy (MTXM) and (b) and (d) Lorentz-TEM (LTEM) techniques. Reciprocal space images measured by the coherent resonant x-ray magnetic scattering (CRXMS) technique show the field-dependent evolution of the magnetic diffraction peaks corresponding to (e) the stripe phase and (f) the skyrmion phase at $T = 210$ K. Integrated intensity measured as a function of the field of the (g) first-order and second-order diffraction spots in the stripe phase and (h) first-order diffraction spots in the skyrmion phase. Schematics in (g) show the transformation of the 1D-CSL from the zero field to the higher field.

structures [18–21]. The sample is grown by DC magnetron sputtering at room temperature at a 3-mTorr Ar pressure with a base pressure of $< 3 \times 10^{-8}$ Torr. Fe and Gd layers were alternatively deposited on a 100-nm thick x-ray transparent Si_3N_4 membrane substrate with 20-nm Ta seed and capping layers [19]. Field-dependent fluctuations that manifest as domain cascades have been observed in those systems along with the presence of critical points and scaling behavior as well as thermally induced spontaneous fluctuations near phase boundaries [18]. These phases are nearly degenerate, and as a result different parts of the phase diagram can be accessed through temperature and applied magnetic fields. The present paper primarily deals with the evolution of the stripe phase as a function of the field at several temperatures. However, our results presented here clearly show that the onset of the dipolar skyrmion phase [20] that changes the dimensionality of the spin system does not exhibit discrete variation of the periodicity in 2D-SkL. It is to be noted here that depending on the initial field protocol the topology of the spin texture

can be changed. That is, the stripe phase can either evolve to a 2D-SkL or to a bubble phase [20,22]. We have used the same [19] field protocol to generate the skyrmion phase in our present paper (refer to Figs. S2(c) and S2 in the Supplemental Material [22]).

Lorentz-TEM images were collected at the University of Oregon using an FEI Titan. Transmission soft x-ray measurements were collected at Beamline 6.1.2 of Advanced Light Source at Lawrence Berkeley National Laboratory, along the Fe L3 (707-eV) absorption edge. Coherent x-ray diffraction measurements were performed also at the Fe L3 edge in Beamline 12.0.2 at the Advanced Light Source as a function of a variable magnetic field applied perpendicular to the sample surface [22]. A small in-plane field (estimated to be 1 mT) comes in our experimental setup due to some trapped field and unavoidable misalignment of the sample-normal with the direction of the applied magnetic field. All measurements were carried out with a linearly polarized x-ray beam. We start our measurement at the zero-field condition and precede to

measure diffraction data as a function of the applied magnetic field at a constant field rate of 1.575 mT/s. A CCD camera placed 0.5 m downstream of the sample was used to record the scattered intensity patterns, which were acquired as a function of the magnetic field over multiple field cycles and repeated at different temperatures.

III. EXPERIMENTAL RESULTS

In Figs. 1(a)–1(d), we show the real-space microscopy images of the stripe and skyrmion phases in a Fe/Gd multilayer film which were obtained using MTXM and LTEM techniques [21]. The LTEM image shows the skyrmion phase of mixed chirality [19,21]. To ascertain if the one-dimensional stripe lattice (1D-SL) in a dipolar system with vanishing DMI does indeed show solitonic behavior, we have employed the reciprocal space technique of coherent resonant CRXMS [18]. Figures 1(e) and 1(f) show the corresponding diffraction pattern observed due to the stripe and skyrmion lattices which enable the determination of domain periodicity as a function of applied magnetic field in the amorphous Fe/Gd multilayer [18,19]. In Fig. 1(e) we show representative CRXMS images of the stripe phase measured at $T = 210$-K temperature exhibiting two symmetric first-order diffraction spots ($Q_1 = \tau$) near zero fields. The intensity of the second-order peak ($Q_2 = 2\tau$) becomes stronger [Figs. 1(e) and 1(g)] with an increase in field and then reduces considerably as the skyrmion phase appears above $H = 200$ mT. The 2D-SkL exhibit sixfold symmetry [refer to Fig. 1(f)] of unequal intensity initially [19], but all the six peaks become almost equal in intensity as H is increased [refer to Fig. 1(h)].

The variation of integrated intensities of different order magnetic peaks provide insight into the phase evolution of the stripe lattice. In Fig. 2, we show the integrated intensity plots of the first- and second-order stripe diffraction spots for four temperatures, viz., 85, 183, 239, and 300 K as a function of the magnetic field. The intensity of the first-order diffraction spot decreases whereas that of the second order increases with the applied magnetic field. Such a variation of intensities in the two peaks is expected as the stripe width of the majority and minority domains changes due to the application of the field. However, in all four representative plots of Fig. 2 intensity of the second peak attain a maximum and then start decreasing as the field approaches critical field H_c above which stripe phase either becomes skyrmion or becomes uniformly magnetized (refer to the phase diagram given in Fig. S1(a) of the SM [22]). Such intensity variation of the first- and second-order peaks with the field has been observed in DMI-based CSL systems [7,16,23,24], and the soliton model represents the measured data very well with only H_c as the fitting parameter. We will show below whereas presenting (refer to Fig. 3) the change in stripe periodicity $L(H,T)$ with the field and temperature in this dipolar interaction mediated thin film also follow the same soliton model as observed [7,14,16] in CSL systems. In this model the elastic-scattering cross section that relates to the scattering intensity of the pth-order diffraction peak is given by [24]

$$I \propto \frac{d\sigma}{d\omega} \sim M^2 \left| J_p^y(\chi) \right|^2 = \left| \frac{\pi^2}{\chi^2 K^2} \frac{Fp}{\cosh(Fp\pi K'/K)} \right|^2. \quad (1)$$
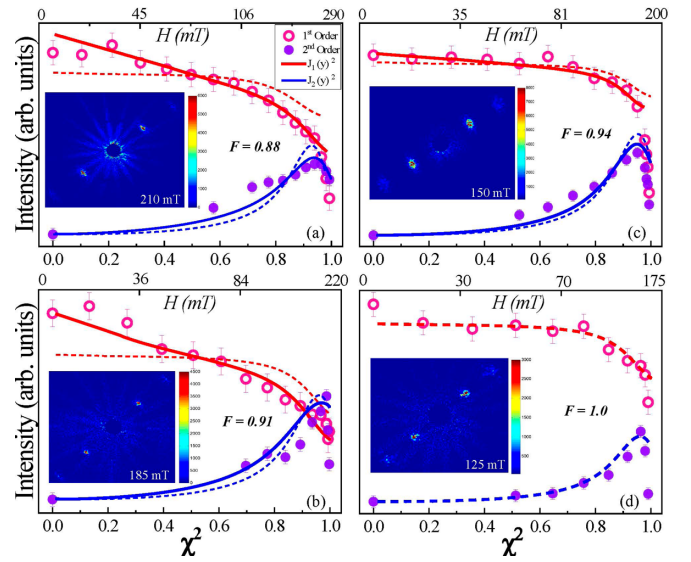

FIG. 2. The field dependence of the integrated intensities for the first- and second-order diffraction spots are shown by pink open circles and violet solid circles, respectively, at (a) $T = 85$ K [$H_c = 256 \pm 3$ mT], (b) $T = 183$ K [$H_c = 200 \pm 2$ mT], (c) $T = 239$ K [$H_c = 192 \pm 2$ mT], and (d) $T = 300$ K [$H_c = 145 \pm 2$ mT] with the corresponding values of H_c as obtained from fitting the data. The inset shows the corresponding 2D diffraction pattern. The solid lines show the theoretical curve with fitting parameter (F) using Eq. (1) and the dotted lines are obtained with $F = 1$.

This expression is obtained using the sine-Gordon equation with $K(\chi)$ and $E(\chi)$, respectively, denoting the elliptic integrals of the first and second kinds with the elliptic modulus χ ($0 \leqslant \chi \leqslant 1$) given by $\chi/E(\chi) = \sqrt{H/H_c}$. Here M is the magnetization and $K' = K(\chi')$ with $\chi' = (1 - \chi^2)^{1/2}$. To obtain a better fit to the experimental data, an additional parameter $F = \sqrt{[L(0,T)/L(0,300)]}$ was used in Eq. (1). Further studies are required to assign the theoretical basis of the parameter F which normalizes stripe periodicity $L(H,T)$ at zero field ($H = 0$) in a given temperature with that obtained at $T = 300$ K. F increases continuously from 0.88 to 1.0 with temperature from 85 to 300 K (refer to the solid lines and dashed lines calculated with $F = 1.0$ in Fig. 2).

The solitonic nature can be further corroborated by studying the stripe periodicity as a function of the field. Most interestingly, we found that the periodicity does not change continuously but in a discrete stepwise manner. In Fig. 3, we show the stripe-periodicity $L(H,T) = 2\pi/Q_1 = 4\pi/Q_2$ of the 1D-SL obtained from the measured values of Q_1 as a function of field H for four representative temperatures. To describe the variation of the stripe periodicity with the field, the same sine-Gordon model [24] that described the field-dependent intensity variation (shown in Fig. 2) was used. $L(H,T)$ can be expressed in terms of $K(\chi)$ and $E(\chi)$ as

$$\frac{L(H,T)}{L(0,T)} = \frac{4K(\chi)E(\chi)}{\pi^2}. \quad (2)$$

The obtained red color curves from Eq. (2) are shown in Figs. 3(a)–3(d) with critical field (H_c) as the only fitting parameter. The measured values of $Q_1 = 2\pi n/\xi(T)$ exhibit
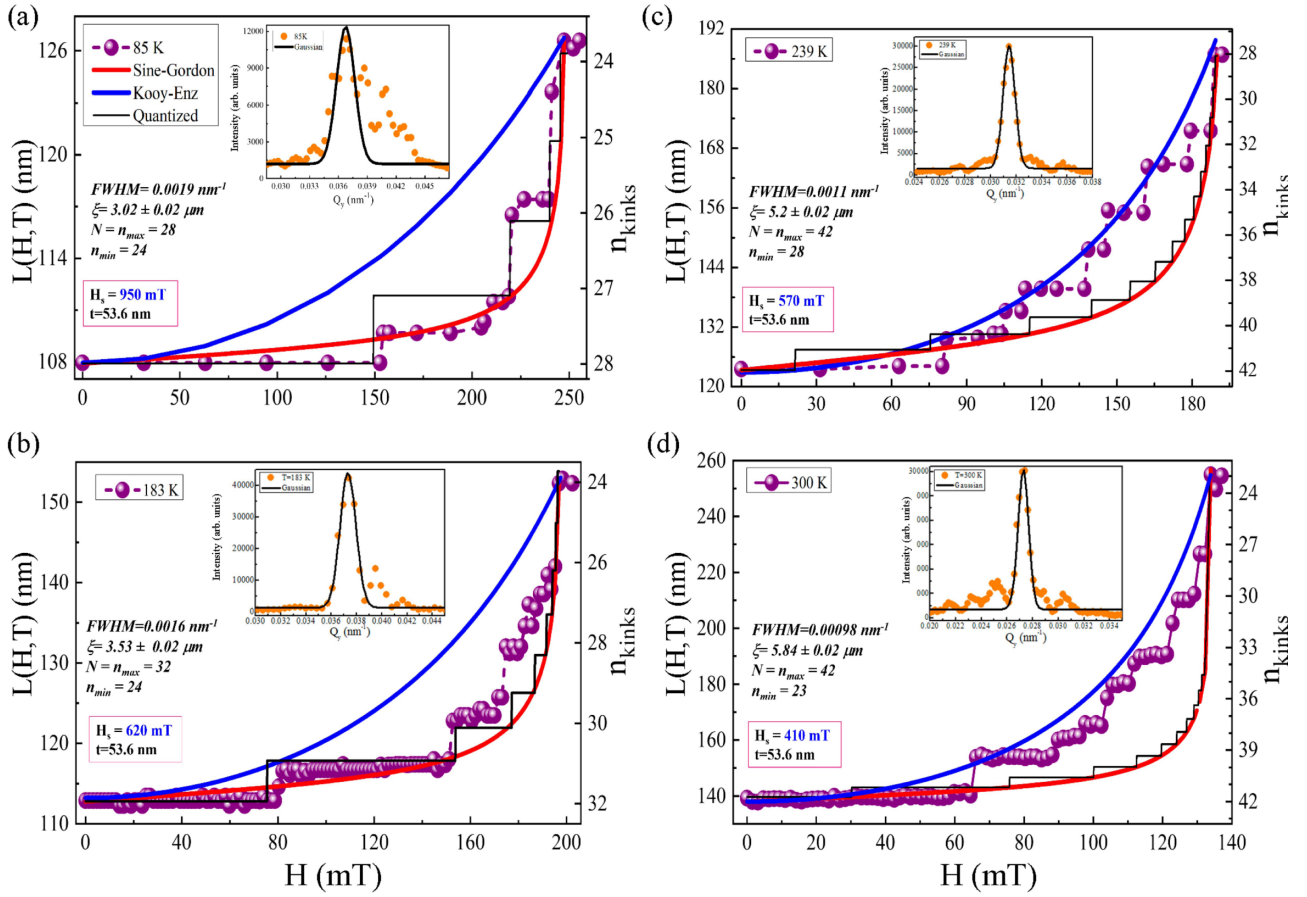
FIG. 3. Experimental plot of the periodicity [$L(H, T)$] at (a) $T = 85$K [$H_c = 249.5 \pm 7$ mT], (b) $T = 183$ K [$H_c = 198.5 \pm 6$ mT], (c) $T = 239$ K [$H_c = 192 \pm 5$ mT], and (d) $T = 300$ K [$H_c = 137 \pm 5$ mT] shown by violet color symbols obtained from diffraction data. The insets displaying plot of intensity vs Q_y shown with orange dots along with their Gaussian fits to extract the full width at half maximum (FWHM) of the magnetic Bragg peaks. The calculated curves shown in red and blue colors are obtained using Eqs. (2) and (3), respectively. Values of the saturation magnetic field (H_s) and the film thickness (t) are shown in each plot. The values of the finite size of the soliton lattice (ξ) having the maximum number of soliton-kinks ($n_{\min}$) represented by "N" and the minimum number of soliton-kinks ($n_{\min}$) at different temperatures are shown inside and right-hand y axis of each plot.

discrete jumps [refer to the inset of Fig. 3(a)] as observed in the CSL of DMI materials [14–16]. In analogy to the CSL material, we consider $\xi(T)$ to represent the finite length of CSL, and it can be estimated from adjacent jumps (ΔQ) of Q_1 corresponding to the the integers "n" and "$n + 1$" giving $\xi(T) = 2\pi/\Delta Q$ at a particular temperature T. The obtained values of $\xi(T)$ is consistent with the value of the FWHM of the measured peak, for example, at 183 K [refer to Fig. 3(b)] $\xi(T) = 0.9 \times 2\pi/\mathrm{FWHM}$ is obtained to be 3.53 μm, which is almost equal to $2\pi/\Delta Q$ with $\Delta Q \approx 0.0018$ nm^{-1} The maximum value of n is N that represents the number of stripes within the finite-size CSL giving $\xi(T)/N = L(0, T)$. With the increasing field, the number of magnetic solitons (spin kinks) represented by n within the finite-size $\xi(T)$ of CSL reduces by integer values [16] and the positions and magnitudes of the quantized jumps could be estimated as $L(H, T)/L(0, T) = N/n$ at all temperatures (refer to the black lines in Fig. 3). Thus, the finite-size $\xi(T)$ which is related to the correlation length of the stripe domains plays a key role for observing this discretized behavior in the stripe periodicity [22]. The number of magnetic solitons (n) at different magnetic

fields ranges from $n_{\max}$ to $n_{\min}$ with decrements of unity (see Fig. 3).

At temperatures above the stripe-to-skyrmion transition temperature (T_c), however, we found that the periodicity $L(H, T)$ changes faster with H than the predicted values of the soliton model. This indicates that the increase in spacing between the solitons results in weaker interaction among solitons which makes the CSL more disordered [6,14,22]. It is reported that at higher temperatures, the stripes get shortened and hybrid skyrmions form that exhibit a complex three-dimensional spin structure that is Bloch-like near the center of the film and more Neel-like near the top and bottom surfaces [25–27]. We, therefore, employ a model that uses the film thickness (t) as a parameter. This model [28,29] can be expressed as

$$\frac{L(H, T)}{L(0, T)} = \sec[\sin^{-1}(h/t)]. \qquad (3)$$

Here $h = H/H_s$ is the reduced field, and H_s is the saturation field [20]. A good agreement with the higher-temperature data can be obtained as shown in Fig. 3. It is worth noting that
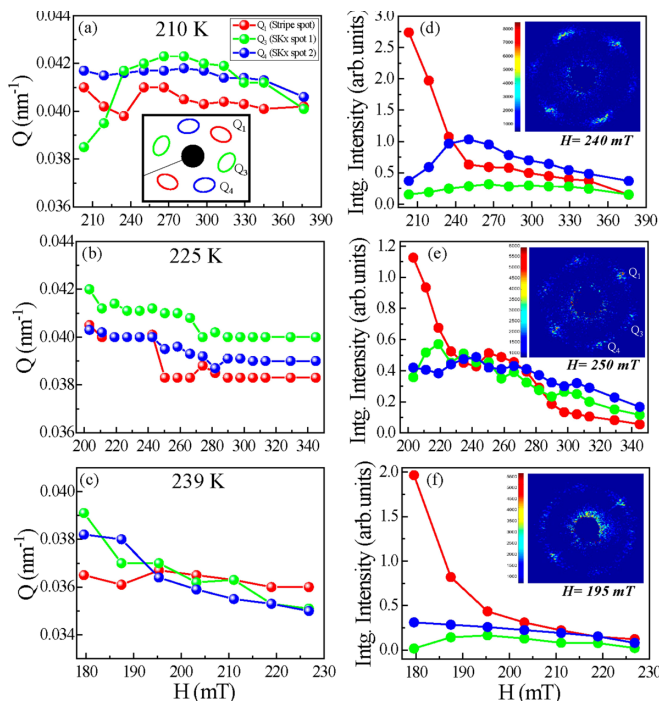
FIG. 4. Evolution of the Q values and the integrated intensities of the first-order diffraction spots in the skyrmion phase at (a) and (d) 210 K, (b) and (e) 225 K, and (c) and (f) 239 K with the magnetic field.

the present scattering geometry is insensitive to the in-plane magnetic spins and the Neel configuration of the spin texture and that allows soliton formalism to represent the intensity variation (refer to Fig. 2) even above stripe-to-skyrmion transition temperature (T_s) quite well.

In Fig. 4, we show the formation process of hexagonal 2D-SkL as a function of field at three different temperatures. All the six spots of 2D-SkL have been marked as red, green, and blue in the inset of Fig. 4(a). At low fields the intensities of the spots are different, however, intensities of Q_1, Q_3, and Q_4 tend to become equal as expected for ideal 2D-SkL with increasing field [refer Figs. 4(a)–4(f)]. At fields between $H = H_c$ and $H = 300$ mT, the positions of the diffraction spots Q_1, Q_3, and Q_4 [see the inset of Fig. 4(a)] remain unequal [19,21]. Interestingly, we do not observe any discrete jump in Q values

of the diffraction spots after skyrmion phase formation (see Figs. 4(a)–4(c)].

IV. CONCLUSIONS

To summarize, the coherent x-ray magnetic scattering results presented here clearly show that 1D-SL in the dipolar-interaction mediated Fe/Gd multilayer behaves, such as a finite-sized chiral soliton lattice as observed in single crystals with dominant DMI [7,30–32]. Discrete jumps in stripe periodicity and intensity variation of first- and second-order satellite diffraction peaks of the stripe lattice follow the soliton sine-Gordon model [24], even though the stripe phase in the Fe/Gd multilayer exhibits an equal population of coexisting and opposite helicity spin stripes. Our results will promote further theoretical and experimental studies to understand the role of local/global chirality and topology in magnetic systems.

[1] R. Wiesendanger, Nat. Rev. Mater. **1**, 16044 (2016).

[2] M.-G. Han, J. A. Garlow, Y. Kharkov, L. Camacho, R. Rov, J. Sauceda, G. Vats, K. Kisslinger, T. Kato, O. Sushkov, Y. Zhu, C. Ulrich, T. Söhnel, and J. Seidel, Sci. Adv. **6**, eaax2138 (2020).

[3] N. Nagaosa and Y. Tokura, Nat. Nanotechnol. **8**, 899 (2013).

[4] A. Fert, N. Reyren, and V. Cros, Nat. Rev. Mater. **2**, 17031 (2017).

[5] X. Z. Yu, N. Kanazawa, Y. Onose, K. Kimoto, W. Z. Zhang, S. Ishiwata, Y. Matsui, and Y. Tokura, Nature Mater. **10**, 106 (2011).

[6] Y. Togawa, T. Koyama, K. Takayanagi, S. Mori, Y. Kousaka, J. Akimitsu, S. Nishihara, K. Inoue, A. S. Ovchinnikov, and J. Kishine, Phys. Rev. Lett. **108**, 107202 (2012).

[7] Y. Okamura, Y. Yamasaki, D. Morikawa, T. Honda, V. Ukleev, H. Nakao, Y. Murakami, K. Shibata, F. Kagawa, S. Seki, T. Arima, and Y. Tokura, Phys. Rev. B **96**, 174417 (2017).

[8] A. O. Leonov and M. Mostovoy, Nat. Commun. **6**, 8275 (2015).

[9] X. Zhang, J. Xia, Y. Zhou, X. Liu, H. Zhang, and M. Ezawa, Nat. Commun. **8**, 1717 (2017).

[10] X. Z. Yu, M. Mostovoy, Y. Tokunaga, W. Zhang, K. Kimoto, Y. Matsui, Y. Kaneko, N. Nagaosa, and Y. Tokura, Proc. Natl. Acad. Sci. USA **109**, 8856 (2012).

[11] B. Göbel, J. Henk, and I. Mertig, Sci. Rep. **9**, 9521 (2019).

[12] X. Z. Yu, Y. Tokunaga, Y. Kaneko, W. Z. Zhang, K. Kimoto, Y. Matsui, Y. Taguchi, and Y. Tokura, Nat. Commun. **5**, 3198 (2014).

[13] H. Barkhausen, Phys. Z **20**, 401 (1919).

[14] Y. Togawa, T. Koyama, Y. Nishimori, Y. Matsumoto, S. McVitie, D. McGrouther, R. L. Stamps, Y. Kousaka, J. Akimitsu, S. Nishihara, K. Inoue, I. G. Bostrem, V. E. Sinitsyn, A. S. Ovchinnikov, and J. Kishine, Phys. Rev. B **92**, 220412(R) (2015).

[15] M. N. Wilson, E. A. Karhu, D. P. Lake, A. S. Quigley, S. Meynell, A. N. Bogdanov, H. Fritzsche, U. K. Rößler, and T. L. Monchesky, Phys. Rev. B **88**, 214420 (2013).

[16] J. I. Kishine, I. G. Bostrem, A. S. Ovchinnikov, and V. E. Sinitsyn, Phys. Rev. B **89**, 014419 (2014).

[17] I. E. Dzyaloshinskiĭ, Sov. Phys. JETP **19**, 960 (1964); **20**, 223 (1965).

[18] A. Singh, J. T. Lee, K. E. Avila, Y. Chen, S. A. Montoya, E. E. Fullerton, P. Fischer, K. A. Dahmen, S. D. Kevan, M. K. Sanyal, and S. Roy, Nat. Commun. **10**, 1988 (2019).

[19] J. T. Lee, J. J. Chess, S. A. Montoya, X. Shi, N. Tamura, S. K. Mishra, P. Fischer, B. J. McMorran, S. K. Sinha, E. E. Fullerton, S. D. Kevan, and S. Roy, Appl. Phys. Lett. **109**, 022402 (2016).

[20] S. A. Montoya, S. Couture, J. J. Chess, J. C. T. Lee, N. Kent, M. Y. Im, S. D. Kevan, P. Fischer, B. J. McMorran, S. Roy, V. Lomakin, and E. E. Fullerton, Phys. Rev. B **95**, 224405 (2017).

[21] J. Chess, S. Montoya, J. Lee, S. Roy, S. Kevan, E. Fullerton, and B. McMorran, Microsc. Microanal. **21**, 1649 (2015).

[22] See Supplemental Material at http://link.aps.org/supplemental/10.1103/PhysRevB.105.094423 for the details of the experimental techniques, scattering geometry in Fig. S1,

for the achiral skyrmion phase shown in Fig. S2 for the determination of the finite-size as given in Sec. IV (Fig. S5), and data analysis schemes.

[23] T. Honda, Y. Yamasaki, H. Nakao, and Y. Murakami, Sci. Rep. **10**, 18596 (2020).

[24] Y. A. Izyumov, Sov. Phys. Usp. **27**, 845 (1984).

[25] R. D. Desautels, L. DeBeer-Schmitt, S. A. Montoya, J. A. Borchers, S. G. Je, N. Tang, M. Y. Im, M. R. Fitzsimmons, E. E. Fullerton, and D. A. Gilbert, Phys. Rev. Material **3**, 104406 (2019).

[26] J. A. Garlow, S. D. Pollard, M. Beleggia, T. Dutta, H. Yang, and Y. Zhu, Phys. Rev. Lett. **122**, 237201 (2019).

[27] W. Legrand, J.-Y. Chauleau, D. Maccariello, N. Reyren, S. Collin, K. Bouzehouane, N. Jaouen, V. Cros, and A. Fert, Sci. Adv. **3**, eaat0415 (2018).

[28] C. Kooy and U. Enz, Philips Res. Rep. **15**, 7 (1960).

[29] V. Gehanno, Y. Samson, A. Marty, B. Gilles, and A. Chamberod, J. Magn. Magn. Mater. **172**, 26 (1997).

[30] V. Ukleev, Y. Yamasaki, O. Utesov, K. Shibata, T. Kanazawa, N. Jaouen, H. Nakao, Y. Tokura, and T.-H. Arima, Phys. Rev. B **102**, 014416 (2020).

[31] S.-G. Je, H.-S. Han, S. K. Kim, S. A. Montoya, W. Chao, I.-S. Hong, E. E. Fullerton, K.-S. Lee, K.-J. Lee, M.-Y. Im, and J.-I. Hong, ACS Nano **14**, 3251 (2020).

[32] J. J. Chess, S. A. Montoya, T. R. Harvey, C. Ophus, S. Couture, V. Lomakin, E. E. Fullerton, and B. J. McMorran, Ultramicroscopy **177**, 78 (2017).